ISPRS Open Journal of Photogrammetry and Remote Sensing 18 (2025) 100104

Contents lists available at ScienceDirect

ISPRS Open Journal of Photogrammetry and Remote Sensing

journal homepage: www.journals.elsevier.com/isprs-open-journal-of-photogrammetry-and-remote-sensing

Global, multi-scale standing deadwood segmentation in centimeter-scale aerial images

Jakobus Möhring [a], Teja Kattenborn [b], Miguel D. Mahecha [a], Yan Cheng [c], Mirela Beloiu Schwenke [d], Myriam Cloutier [e], Martin Denter [f], Julian Frey [g], Matthias Gassilloud [b,f], Anna Göritz [b,f], Jan Hempel [a], Stéphanie Horion [c], Tommaso Jucker [h], Samuli Junttila [i], Pratima Khatri-Chhetri [j], Kirill Korznikov [k], Stefan Kruse [l], Etienne Laliberté [m], Michael Maroschek [n,o], Paul Neumeier [a], Oscar Pérez-Priego [p], Alastair Potts [q], Felix Schiefer [r], Rupert Seidl [n,o], Janusch Vajna-Jehle [b], Katarzyna Zielewska-Büttner [s], Clemens Mosig [a,*]

[a] Institute for Earth System Science and Remote Sensing, Leipzig University, Germany
[b] Chair of Sensor-based Geoinformatics (geosense), University of Freiburg, Germany
[c] Department of Geosciences and Natural Resource Management, University of Copenhagen, Denmark
[d] Department of Environmental Systems Sciences, ETH Zurich, Switzerland
[e] Department of Forest and Conservation Sciences, University of British Columbia, Canada
[f] Chair of Remote Sensing and Landscape Information Systems, University of Freiburg, Germany
[g] Chair of Forest Growth and Dendroecology, University of Freiburg, Germany
[h] School of Biological Sciences, University of Bristol, UK
[i] Department of Forest Sciences, University of Helsinki, Finland
[j] School of Environmental and Forest Sciences, University of Washington, USA
[k] Department of Functional Ecology, Institute of Botany of the Czech Academy of Sciences, Czechia
[l] Polar Terrestrial Environmental Systems, Alfred Wegener Institute Helmholtz Centre for Polar and Marine Research, Potsdam, Germany
[m] Département de sciences biologiques, Université de Montréal, Canada
[n] Research and Monitoring, Nationalpark Berchtesgaden, Germany
[o] TUM School of Life Sciences, Technical University of Munich, Germany
[p] Department of Forestry Engineering, University of Cordoba, Spain
[q] Spekboom Restoration Research Group, Botany Department, Nelson Mandela University, South Africa
[r] Institute of Geography and Geoecology, Karlsruhe Institute of Technology (KIT), Germany
[s] Department of Forest Nature Conservation, Forest Research Institute (FVA), Germany

ARTICLE INFO

Dataset link: https://deadtrees.earth/

Keywords:
Standing deadwood
Aerial images
Orthophotos
Centimeter-scale images
Remote sensing
Tree mortality

ABSTRACT

With tree mortality rates rising across many regions of the world, efficient methods to map dead trees are becoming increasingly important to monitor forest dieback, assess ecological impacts, and guide management strategies. Deep learning-based pattern recognition combined with the high spatial detail of aerial images from drones or airplanes provides an avenue for mapping dead tree crowns or partial canopy dieback, collectively referred to as standing deadwood. However, current methods for mapping standing deadwood are limited to specific biomes or image resolutions. Here, we present a transformer-based semantic segmentation model that generalizes across forest biomes and a wide range of image resolutions (1–28 cm) for mapping both dead tree crowns and partial canopy dieback. Our approach combines a SegFormer-based transformer architecture for image feature extraction and Focal Tversky Loss to mitigate class imbalance. We used a globally distributed crowd-sourced dataset of 434 high-resolution aerial images and manual delineations of standing deadwood of vastly varying quality. The orthophotos span all major forest biomes and cover 10,778 hectares. To further mitigate imbalances across biomes, resolutions, deadwood occurrence, and image sources, we developed a four-dimensional sampling scheme that ensures balanced representation during training. The models were trained and evaluated using heterogeneous crowd-sourced data, which, as expected, negatively affects the F1-scores.

* Corresponding author.
E-mail address: clemens.mosig@uni-leipzig.de (C. Mosig).

https://doi.org/10.1016/j.ophoto.2025.100104
Received 12 May 2025; Received in revised form 7 October 2025; Accepted 8 October 2025
Available online 21 October 2025

A visual inspection on independent data highlights the very precise quality of the segmentation. Our analysis revealed resolution-dependent performance variations across biomes, suggesting a relationship between optimal mapping resolution and biome-specific characteristics. We make both our model and a machine-learning-ready dataset publicly available on deadtrees.earth to support future research in tree mortality mapping.

1. Introduction

In recent years, elevated tree mortality has been observed in many regions of the world (Hartmann et al., 2022; Trumbore et al., 2015; Allen et al., 2015). Our ability to understand and quantify tree mortality dynamics remains limited, as there is a lack of comprehensive, globally applicable data and assessment methods. Developing effective methods for assessing tree mortality across forest types and biomes is crucial for a consistent monitoring and informing forest management strategies from regional to global scales (The International Tree Mortality Network et al., 2025).

Remote sensing has proven highly effective for mapping standing deadwood canopies at local to regional scales. In particular, aerial imagery, when combined with deep-learning-based segmentation algorithms, provides a powerful means to map dead crowns (Kattenborn et al., 2021; Schiefer et al., 2023; Cheng et al., 2024; Khatri-Chhetri et al., 2024). Such pattern recognition algorithms can detect characteristic spatial features of dead tree crowns to locate or segment dead tree crowns. For example, Cheng et al. (2024) applied instance segmentation to RGB-NIR airplane imagery across California and achieved individual dead tree detection accuracies of 80%–90%. In the same region, Khatri-Chhetri et al. (2024) showed for a semantic segmentation of tree crowns very high-resolution RGB imagery (0.1 m) yielded superior performance (F_1 = 0.76) compared to 1 m hyperspectral imagery (F_1 = 0.69) or 0.6 m RGBNIR imagery (F_1 = 0.61). At even finer resolutions (2–4 cm), Schiefer et al. (2020, 2023) demonstrated that drone-based orthophotos, together with semantic segmentation, enable robust mapping of dead canopies (F_1 = 0.75, 0.85) ranging from entire crowns down to individual branches.

The demonstrated effectiveness of RGB aerial imagery for mapping standing deadwood builds on two key properties. First, dead crowns and leafless branches lack green foliage and therefore appear in distinctive gray–brown tones that contrast sharply with the green canopies of living trees (Schiefer et al., 2023). Second, RGB imagery provides the highest spatial detail compared to other spectral regions, because the sun emits most of its energy in the visible domain, enabling high signal-to-noise ratios, shorter exposure times, and ultimately sharper images (Khatri-Chhetri et al., 2024; Kattenborn et al., 2021). While RGB airplane imagery is very effective for large scale assessments, drone orthophotos with centimeter-scale resolution are particularly promising, as their fine spatial detail enables capturing entire dead tree crowns but also early and partial canopy dieback (Mosig et al., 2024; Schiefer et al., 2023).

Despite these growing capabilities, current approaches for harnessing RGB imagery remain fragmented. Most studies are restricted to either drone or airplane imagery, to specific spatial resolutions, or to particular forest types and regions. As a result, existing models are highly specialized and often lack transferability beyond their original training context (Khatri-Chhetri et al., 2024; Cheng et al., 2024; Schiefer et al., 2023; Junttila et al., 2024; Schwarz et al., 2024; Allen et al., 2024). Yet, to advance operational and consistent monitoring of forest mortality we require transferable computer vision models that can seamlessly integrate imagery from both drones and airplanes, generalize across biomes, and capture the full spectrum of canopy decline, from early-stage partial dieback to fully dead tree crowns (The International Tree Mortality Network et al., 2025).

Several factors complicate the training of a generalizable computer vision model for detecting standing deadwood in aerial images. One major challenge lies in the high variability of visual tree characteristics, such as leaf morphology, branching architecture, and crown geometry, which differ substantially across biomes and species (Mosig et al., 2024; Jucker et al., 2024). This variability is particularly pronounced in forest types dominated by broadleaved species, which typically exhibit more complex crown structures and multilayered canopies compared to coniferous forests (Zielewska-Büttner et al., 2020). As a result, detecting tree mortality is especially difficult in tropical, dryland, and deciduous temperate forest ecosystems (Schiefer et al., 2023; Cheng et al., 2024). Additionally, open-canopy forests — such as those in dryland, boreal, or montane regions — pose further challenges. In these systems, visually similar features like bare soil, dead understory vegetation, or coarse woody debris may be confused with standing dead trees, complicating accurate detection.

Another challenge lies in the nature of the aerial imagery. Sensor characteristics — such as focal length, shutter type, and resolution — as well as operational conditions like flight speed and wind, can impact the visual appearance of tree canopies and the performance of image-matching techniques (Frey et al., 2018; Denter et al., 2022), and computer vision models (Kattenborn et al., 2021). Aerial imagery can range in resolutions from less than 1 cm, in drone flights, to 30 cm or even 60 cm in airplane imagery (see https://github.com/YanCheng-go/open-aerial-photos). To manage this variability, aerial images are commonly resampled to a unified resolution (Schiefer et al., 2023). However, this process can discard potentially valuable information relevant to tree mortality detection. Also, image processing — particularly the ortho-rectification process, which aligns and projects overlapping top-down images into an orthophoto — can introduce minor distortions in the resulting orthophotos. Lastly, the illumination conditions during the data acquisitions, such as cloud cover, atmospheric composition, and related scattering properties can introduce a substantial variability in the appearance of plant canopies, which can affect the transferability of pattern recognition models (Kattenborn et al., 2022). These factors collectively present significant challenges in training and applying generic segmentation models to identify standing deadwood in aerial images.

Training a robust segmentation model for standing deadwood requires a comprehensive dataset covering the above-described variations in image and vegetation properties. Fortunately, the availability of orthophotos is rapidly expanding, and there is a growing momentum among researchers and institutions to openly share these data (Mosig et al., 2024). The largest, crowd-sourced orthophoto repository for the forest domain is the deadtrees.earth initiative, which hosts over 3000 individual datasets contributed by more than 300 collaborators from over 100 institutions. This extensive collective dataset consists of aerial images from drones and airplanes across all biomes and major forest types, where standing deadwood delineations were provided for a subset of orthophotos. Here, we leverage this crowd-sourced dataset using a tailored data sampling and image rescaling approach to train a generalizable semantic segmentation model based on a vision transformer architecture. This model is designed to map standing deadwood across different image resolutions from 1 to 28 cm and all major biomes. We demonstrate its ability to identify deadwood features ranging from partial canopy dieback to fully dead tree crowns. Moreover, by testing the model with independent orthophotos across all biomes, we demonstrate that the model generalizes across different biomes, forest types, and image characteristics. Beyond developing a generalizing semantic segmentation model, a key contribution of this study is a publicly available, machine-learning-ready tiled dataset for multi-scale cross-biome mapping of tree mortality. This dataset and the trained model provide the first benchmark opportunities and baseline for evaluating globally transferable segmentation models for deadwood detection.

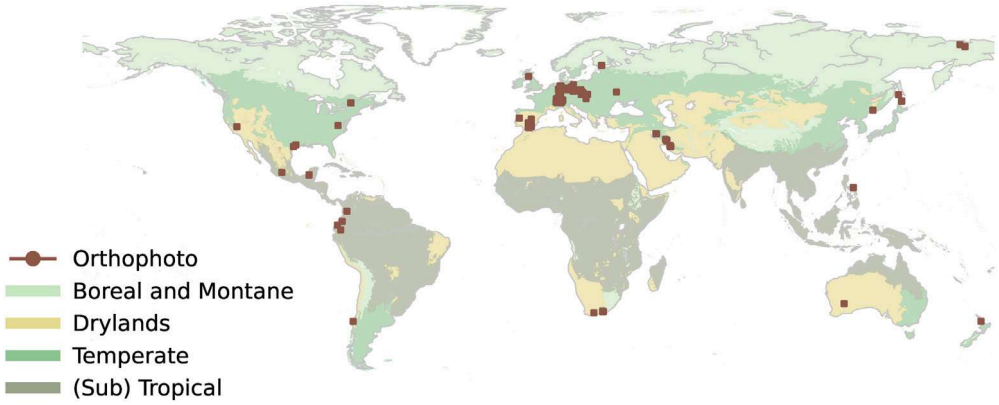

Fig. 1. Locations of manually labeled orthophotos. Background colors denote aggregated biome groups based on Olson et al. (2001). (For interpretation of the references to color in this figure legend, the reader is referred to the web version of this article.)

2. Dataset

For this study, we extracted all orthophotos with manual labels from deadtrees.earth, distributed across all major forested biomes (Mosig et al., 2024). The deadtrees.earth database provides high-resolution aerial images collected from drones and airplanes, where a subset includes manual segmentation labels. We only selected a subset of images with resolutions finer than or equal to 28 cm, as a prior analysis did not indicate promising results beyond this image resolution. Additionally, we extracted the labels from deadtrees.earth, which are manual delineations of dead tree crowns or partial canopy dieback (leafless branches) based on visual interpretation. Given the crowd-sourced nature of these labels from various researchers, deadtrees.earth categorized the labels into three groups by quality, that is, low, medium, and high (Mosig et al., 2024). We only used those with medium or high quality. High-quality labels precisely delineate the shape of dead trees as detailed polygons, capturing fine features such as dead branches. Medium-quality labels provide only approximations, typically as simple circles, and may not capture partial dieback. Labels that are highly inaccurate and unsuitable for effective model training are considered low-quality. Including these medium-quality datasets was necessary to ensure coverage across all ecosystems, but it is important to consider during the later model performance assessment, as the limited precision of the labels may lead to lower evaluation scores even when the model performs accurately or better than the labels themselves. Lastly, each set of orthophotos and labels includes a polygon defining the area of interest. This is the region within the orthophoto where all visible dead trees, and in some cases partial dieback, were labeled as standing deadwood. Areas outside the area of interest are excluded from model training and evaluation.

The final dataset selected for model training and performance assessment consists of 434 sets of orthophotos and labels, covering a total labeled area of 10,778 hectares across all forested biomes. We assigned each image to a biome using the intersection of the orthophoto centroid with the biome boundaries defined by Olson et al. (2001). All original biomes by Olson et al. (2001) were then aggregated into coarser biome groups for simplicity (see Appendix A.1). The resulting four biome groups were (1) (sub) tropical, (2) boreal and montane, (3) drylands (including Mediterranean), and (4) temperate forests (see Fig. 1). Given its broad coverage, the deadtrees.earth dataset encompasses substantial variation in biome-specific characteristics. Different biomes inherit diverse visual characteristics across the datasets regarding tree species diversity, understory vegetation, and forest floor properties.

For example, orthophotos from dense temperate broadleaf and mixed forests can provide a clear visual distinction of dead and alive canopies, as standing deadwood is easily distinguishable against the darker canopy of intact trees (Fig. 2, top). In contrast, in open forests or for less dense tree crowns of drylands or Mediterranean forests, a bright ground often results in lower contrast with dead vegetation and can challenge the detection of dead trees (Fig. 2, bottom). These contrasts underscore that cross-biome heterogeneity in visual appearance is essential for training and fairly evaluating segmentation models that are robust and transferable.

Table 1
Dataset distribution across biomes. Resolution is computed per orthophoto and then averaged per biome group. Label quality is a categorical value of 1 (low quality, not present), 2 (medium quality), or 3 (high quality), reported per orthophoto (Mosig et al., 2024) and averaged by biome. std. = standard deviation, Res. = image resolution.

Biome group	Orthophoto [N]	Mean label quality	Mean Res. (std.) [cm]	Mean area (std.) [ha]
(Sub) Tropical	9	2.78	4.20 (1.90)	34.65 (28.64)
Boreal and Montane	11	2.55	3.15 (2.16)	8.54 (9.73)
Drylands	97	2.11	20.35 (9.28)	48.30 (300.24)
Temperate	317	2.71	4.52 (6.18)	17.94 (57.41)
Total	434	2.57	8.02 (9.54)	24.83 (150.25)

Building on diverse community contributions to the deadtrees.earth database, the dataset used here captures a broad spectrum of image resolutions and spatial extents, which provides valuable variability for model development. Specifically, the dataset includes a wide variation of different image resolutions, ranging from 1 cm to 26.2 cm. Images acquired by drones typically have resolutions between 1 cm and 5 cm, given a common operating height between 60 and 120 m above ground level, and now widely available 4K RGB image sensors. Older images and these from public aerial surveys typically have an image resolution coarser than 10 cm, which only suffices for reliable standing deadwood detection in a subset of biomes and may not unveil partial dieback (Mosig et al., 2024). Within biome groups, we also observed large variations in the orthophoto footprint size (see Table 1). For example, the drylands biome group contains a single orthophoto of 2500 ha, while the mean footprint is 48.3 ha for this biome. This uneven distribution of orthophoto resolutions and coverage exacerbated the stark uneven geographic distribution already present across biome groups.

3. Methods

3.1. Data preprocessing

To prepare the aerial images and standing deadwood labels for semantic segmentation, we applied a series of preprocessing steps, including rasterization, reprojection, rescaling, and tiling. Each of these steps is critical in transforming the raw data into a format suitable for

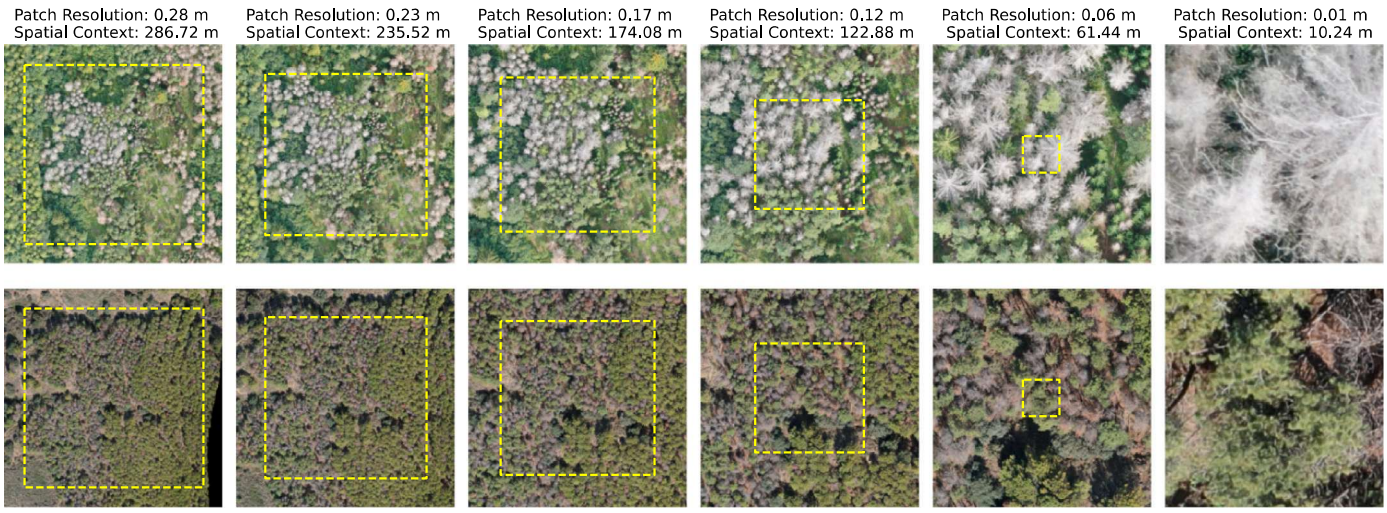

Fig. 2. Comparison of fixed tile sizes (1024 pixels) across the target range of resolutions. Yellow boxes outline the extent of the tile for the next resolution. (For interpretation of the references to color in this figure legend, the reader is referred to the web version of this article.)

training a segmentation model that generalizes across a wide range of common drone-shot image resolutions.

Label rasterization. The vector polygons delineating standing deadwood were transformed into raster images, where standing deadwood was assigned the value 1 and background the value 0, creating pixel-level masks of the original image, using the original spatial resolution of the associated image. Additionally, we added a placeholder for areas outside the area of interest, denoted by the value 255. These areas are excluded from the loss calculation and evaluation in later steps, allowing us to process tiles that contain areas outside the area of interest without penalizing the model.

Reprojection. To standardize the spatial reference of the aerial images, we reprojected all orthophotos and masks to the respective Universal Transverse Mercator (UTM) zone that was derived based on the WGS84 centroid of each orthophoto. Each UTM coordinate reference system is only valid for specific regions on Earth but minimizes distortion and maximizes distance precision. Furthermore, the unit of the coordinate reference system is meters allowing straightforward and precise calculation of the image resolution and facilitating down-scaling to other lower resolutions.

Rescaling. As a result of different flight heights and sensors, aerial images from drones and airplanes are acquired at different resolutions. Therefore, we augmented our dataset with a progressive down-scaling of the images and masks (Fig. 2). This rescaling is crucial for the generalization capabilities of our segmentation model. By providing more training examples at different resolution levels, it enables the model to perform accurately across various scales. We incrementally downscaled the images and masks to a fixed set of resolutions between 2 cm and 28 cm per pixel in 2 cm steps. This means an orthophoto with an original resolution of 14.5 cm was downscaled to 16, 18, ..., 26 cm. The orthophoto and mask at its original resolution and the resampled versions were then used for further analysis.

Tiling. The segmentation model (described below) requires all images and masks to be represented in a consistent shape. The rescaled orthophotos and masks were divided into tiles of 1024 × 1024 pixels. For the lowest resolutions of 1 cm, this ensures a spatial context of 10.24 m (Jucker et al., 2022). The tiles were extracted with an overlap of 50% across orthophotos, increasing the amount of available training data. Lastly, we removed tiles from the dataset that have more than 80% no data values. While it may be intuitive to purge tiles without standing deadwood in preprocessing, they are necessary during training for the model to generalize across non-vegetated areas, such as non-forest areas or healthy forests.

3.2. Sampling

The orthophotos and derived tiles are unevenly distributed across biome groups, resolutions, standing deadwood occurrence, and orthophotos (see Section 2). Additionally, the rescaling process exacerbates the imbalance across image resolutions. This happens because fewer low-resolution tiles can be generated from the same orthophoto, as they cover larger areas. To counteract these imbalances we implemented a multi-dimensional sampling process.

In each training epoch, the dataset was grouped by biome group, resolution bin, and a binary standing deadwood attribute that indicates whether at least one pixel in the tile represents standing deadwood. This resulted in 112 groups, calculated as follows:

$$4(\text{biome gr.}) \cdot 14(\text{res. bins}) \cdot 2(\text{deadwood}) = 112$$

To avoid the over-representation of tiles from larger orthophotos, we randomly selected a maximum of 50 tiles per orthophoto within each group. We then selected 100 random tiles per group, and oversampled when fewer than 100 tiles were available. This process yielded $112 \times 100 = 11200$ training tiles per epoch.

3.3. Segmentation model setup

U-Net has become one of the most widely used model architectures for semantic segmentation, largely because it consistently outperforms traditional convolutional neural networks. Its strength lies in its ability to efficiently and accurately localize features, even when input tile sizes vary (Ronneberger et al., 2015). The model uses an encoder–decoder structure, where the encoder compresses the input into a compact set of features, while the decoder reconstructs a segmentation map. One key advantage of this design is that the encoder part of the model can be interchanged with different model structures.

Based on this, recent work by Veitch-Michaelis et al. (2024) showed that using a transformer-based SegFormer encoder for semantic segmentation yielded very promising results. Following this approach, we chose the largest SegFormer variant (B5), which has about 81 million trainable parameters and performed best in general tree segmentation. The resulting model consists of a SegFormer-B5 encoder, pretrained on ImageNet, paired with the standard U-Net decoder implemented using the `segmentation_models.pytorch` library (Iakubovskii, 2019). In total, the model, including the encoder and decoder parts, consists of 84.7 million trainable parameters. For training, we used the AdamW optimizer, which is a widely used optimizer in computer vision applications (Loshchilov, 2017). We trained the segmentation

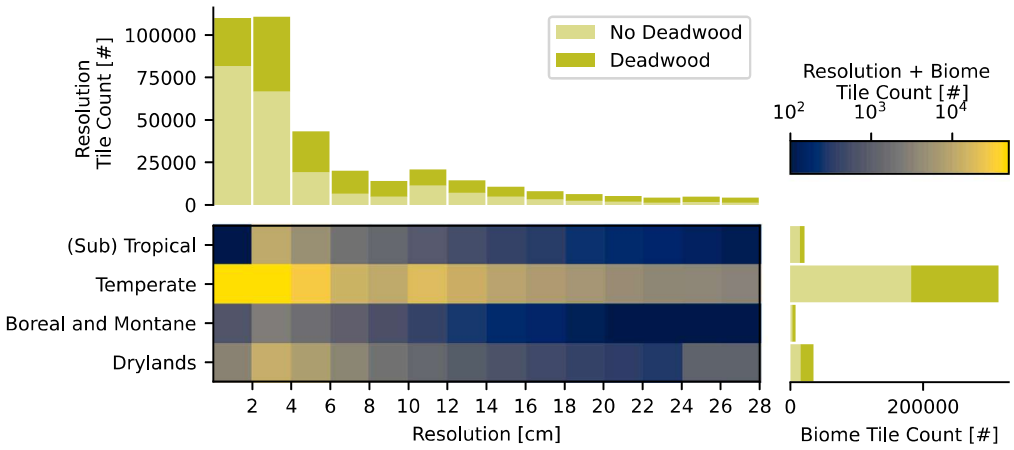

Fig. 3. Distribution of tiles after tiling across resolution (2–28 cm) and biome groups. Resolutions are grouped into bins, where the resolution indicates the upper bound of the bin. The heatmap is log-scaled. The upper histogram denotes the distribution across resolutions, and the right histogram across the major forest biomes. The histograms are split into tiles containing at least one pixel of standing deadwood and tiles without any standing deadwood.

model with PyTorch (Paszke et al., 2019), alongside Hugging Face's Accelerate library (Gugger et al., 2022), which exposes a high-level API for distributed training of the segmentation model, allowing it to be trained on multiple GPUs with little implementation effort.

We incorporated dynamic data augmentation steps performed during model training, including random vertical and horizontal flipping of both the image and its corresponding segmentation mask, along with random contrast adjustments to the image. These augmentations help prevent the model from memorizing specific training examples and enhance its ability to generalize across varying lighting conditions in the imagery. The model takes batches of the augmented image tiles as input and outputs continuous masks, which are converted into a probability distribution via a sigmoid layer. To obtain a binary mask from the probabilities, we classified pixels with probabilities $p \geq 0.5$ as standing deadwood.

The model was trained for 105 epochs. The learning rate was initially set to 10^{-9} and linearly warmed up to 10^{-5} over the first 15 epochs, after which it was maintained at 10^{-5}. A weight decay of 10^{-4} was applied throughout training.

For computational efficiency, we utilized the `fp16` floating-point format, which reduces precision while significantly accelerating training due to its smaller bit size (16 bits compared to 32 in `fp32`). Unlike `fp16`, which also uses 16 bits, `bf16` allocates 8 bits to the exponent (compared to 5 in `bf16`), enabling it to represent larger gradients. We used three NVIDIA A6000 GPUs in parallel with a batch size of four per GPU, thus 12 tiles in total.

3.4. Loss function

Class imbalance within a tile is a common challenge in segmentation tasks. Here, it originated from the natural disproportion between standing deadwood and the background pixels in the imagery. This imbalance is exacerbated by scattered mortality, often made up of only a dozen of pixels per dead tree in low-resolution tiles. This is particularly problematic when evaluating model performance, as traditional metrics like accuracy become misleading. For example, if 97.5% of the pixels belong to the background class, a model that predicts only background pixels — ignoring standing deadwood entirely — would still achieve a high overall pixel accuracy of 0.975. While this may result in high overall accuracy, it would lead to poor recall for the minority class (standing deadwood).

To address this issue, we employ Focal Tversky Loss, as recommended by Jadon (2020). The Focal Tversky Loss (Abraham and Khan, 2019) is derived from the Tversky Index (TI), which generalizes the widely used Dice Score Coefficient. The Dice Score Coefficient is a common metric for evaluating the overlap between predicted segmentation maps and reference labels, and it is mathematically equivalent to the F1-score (Müller et al., 2022). A limitation of the Dice Score Coefficient is that it penalizes false positives (background classified as standing deadwood) and false negatives (standing deadwood classified as background) equally. Since background pixels are far more abundant in our case, this can cause the model to favor negative predictions, leading to poor performance on the minority class (standing deadwood). The TI addresses this by introducing the weighting parameters α and β, which allow the asymmetric penalization of false positives and false negatives, depending on the chosen configuration. When $\alpha = \beta = 0.5$, the TI reduces to the Dice Score Coefficient. TI can be described as follows:

$$TI = \frac{\sum(y \cdot \hat{y}) + \epsilon}{\sum(y \cdot \hat{y}) + \alpha \cdot \sum((1-y) \cdot \hat{y}) + \beta \cdot \sum(y \cdot (1-\hat{y})) + \epsilon}$$

where y represents the standing deadwood probability of the reference data, and $\hat{y}$ is the predicted probability. To maintain numerical stability when the reference probability approaches zero, a small constant ϵ is added to the equation. The Tversky Loss (TL) is defined as $TL = (1-TI)$. Further, the Focal Tversky Loss (FTL) introduces a modulation parameter γ, adjusting the focus on difficult samples: $FTL = (1-TI)^{\gamma}$. When γ is greater than one, samples with a high TI — indicating accurate predictions — contribute less to the overall loss due to the nonlinear relationship between TI and loss. In our case, a $\gamma > 1$ is preferable to focus on harder-to-learn examples and to achieve a steeper gradient on examples where segmentation performance is lacking.

We incorporated the area of interest in the training process to ensure that the loss is only applied in labeled areas of the image. We modified the Focal Tversky Loss implementation to incorporate a weight mask, which sets the loss to zero outside the area of interest. We determined $\alpha = 0.2$, $\beta = 0.8$ and $\gamma = 2$ as the parameters of the Focal Tversky Loss based early experiments optimizing the trade-off between precision and recall.

3.5. Evaluation

We evaluated the model by computing the number of true positives (TP), false positives (FP), and false negatives (FN) for the standing deadwood class for each tile. Depending on the subsequent analysis, these pixel-based metrics were summed across groups (e.g., biome or resolution) of tiles and used to calculate the Precision (Eq. 3.5), Recall (Eq. 3.5) and F1-score (Eq. 3.5).

$$\text{Precision} = \frac{\text{TP}}{\text{TP} + \text{FP}}$$

$$\text{Recall} = \frac{\text{TP}}{\text{TP} + \text{FP}}$$

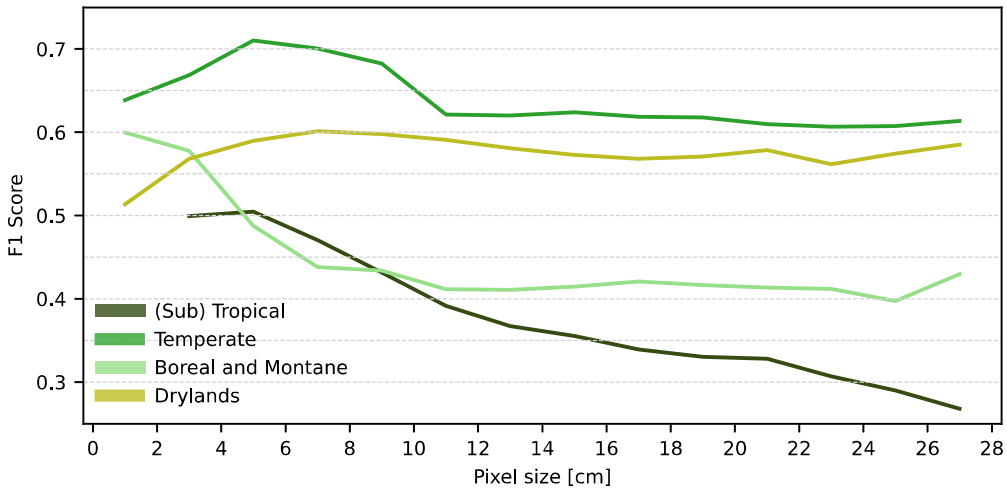

Fig. 4. Mean F1-scores derived from the 3-fold spatial block cross-validation across biome groups and resolution bins. Note that F1-scores are obtained from heterogeneous and crowd-sourced labels and hence represent a conservative model performance estimate.

Table 2
F1-score, precision, and recall across biomes, for the respective best performing resolution.

Biome group	F1-score	Precision	Recall
(Sub) Tropical	0.51	0.40	0.69
Temperate	0.71	0.59	0.90
Boreal and Montane	0.60	0.48	0.81
Drylands	0.60	0.47	0.83

$$\text{F1-score} = 2 \times \frac{\text{Precision} \times \text{Recall}}{\text{Precision} + \text{Recall}}$$

To robustly estimate the performance of the trained segmentation model, we employed a 3-fold spatial block cross-validation strategy, where each orthophoto is considered a spatial block. This prevents an overestimation of the model performance due to spatial autocorrelation (Kattenborn et al., 2022). For evaluation, the last epoch (105) was chosen in all folds as training has fully converged here. No dynamic model selection or hyperparameter tuning was performed due to computational constraints. The trained segmentation models were finally evaluated based on the combined independent cross-validation sets.

To visualize the resulting predictions as vectors and enable their use in other applications, we used the function `findContours` in the OpenCV Python library (Bradski, 2000) to convert the raster predictions with a pixel value of ≥0.5 into polygons. The chosen algorithm supports the generation of both outer contours and interior holes. A single polygon corresponds to a contiguous deadwood area, which can correspond to a single dead branch, partial dieback, a fully dead tree, or a group of dead trees.

4. Results

The multi-step sampling scheme across biome group, resolution bin, and presence of deadwood pixels resulted in a total of 378,430 pairs of image tiles and their corresponding binary standing deadwood masks. The distribution of the generated tiles was highly skewed towards high-resolution tiles in temperate regions (see Fig. 3). Temperate biomes and images with resolutions better than 4 cm were by far the most present examples. The smallest amount of training data was available for the boreal and montane biomes and for tropical regions. Low-resolution images were significantly underrepresented due to the sampling scheme and the real-world size of the labeled area that is required to obtain one low-resolution tile with a width and height of 1024 pixels. Lastly, across biome groups and resolution bins, tiles without any standing deadwood were generally more frequent than with standing deadwood.

With spatial block cross-validation, the highest F1-score of 0.71 was achieved for temperate biomes and the lowest of 0.51 for tropical regions (Table 2). The highest precision and recall were received for temperate forests, for which also the most amount of training data was available (see Fig. 3). The recall generally was 52.5% to 76.6% higher than the precision with 90% of standing deadwood pixels recovered in temperate forests. This yielded a mean F1-score performance of 0.61, averaged across biomes.

We found that the segmentation performance was inconsistent across resolutions (Fig. 4). In most cases, lower resolutions which contain less spatial detail, yielded comparably worse performance. However, for Temperate and Dryland biome groups, we observed an optimal resolution range for standing deadwood segmentation between 4 cm and 8 cm. Here, the highest resolution bin (≤2 cm) yielded worse performance, on par with the much lower resolutions. The results for boreal and montane biomes did not follow this trend, and show almost exclusively a consistent decline in performance with coarser resolutions.

An additional qualitative evaluation of the predictions, based on visual interpretation of independent, crowd-sourced orthophotos from deadtrees.earth, revealed precise segmentation of standing deadwood and partial dieback in orthophotos (Fig. 5). Often, the predictions exceeded the segmentation quality and completeness of the labels. Moreover, this evaluation revealed several instances where predictions were true positives, while labels for an actual presence of standing deadwood or partial dieback were absent.

5. Discussion

We demonstrated the generalization of a segmentation model for segmenting standing deadwood including fully dead tree crowns and partial canopy dieback in orthophotos across biomes and resolutions from 2 to 28 cm.

The results suggested an optimal resolution for each biome, and the finest resolutions have generally not shown the highest performance. This could be explained by the fact that finer resolutions at a fixed tile size yield tiles with a smaller spatial extent (Fig. 2). This is in line with Schiefer et al. (2020), who found that the amount of real-world spatial context and finer resolutions do not necessarily result in better accuracies. This would suggest that models trained with a tile size that is larger than 1024 pixels, which was used in this study, *e.g.,* 2048 pixels, would show a different optimal resolution. Another possible explanation for an optimal resolution is a link to tree crown architecture which varies heavily across biomes (Jucker et al., 2022). For example, in the boreal, mountain and temperate biomes tall forests

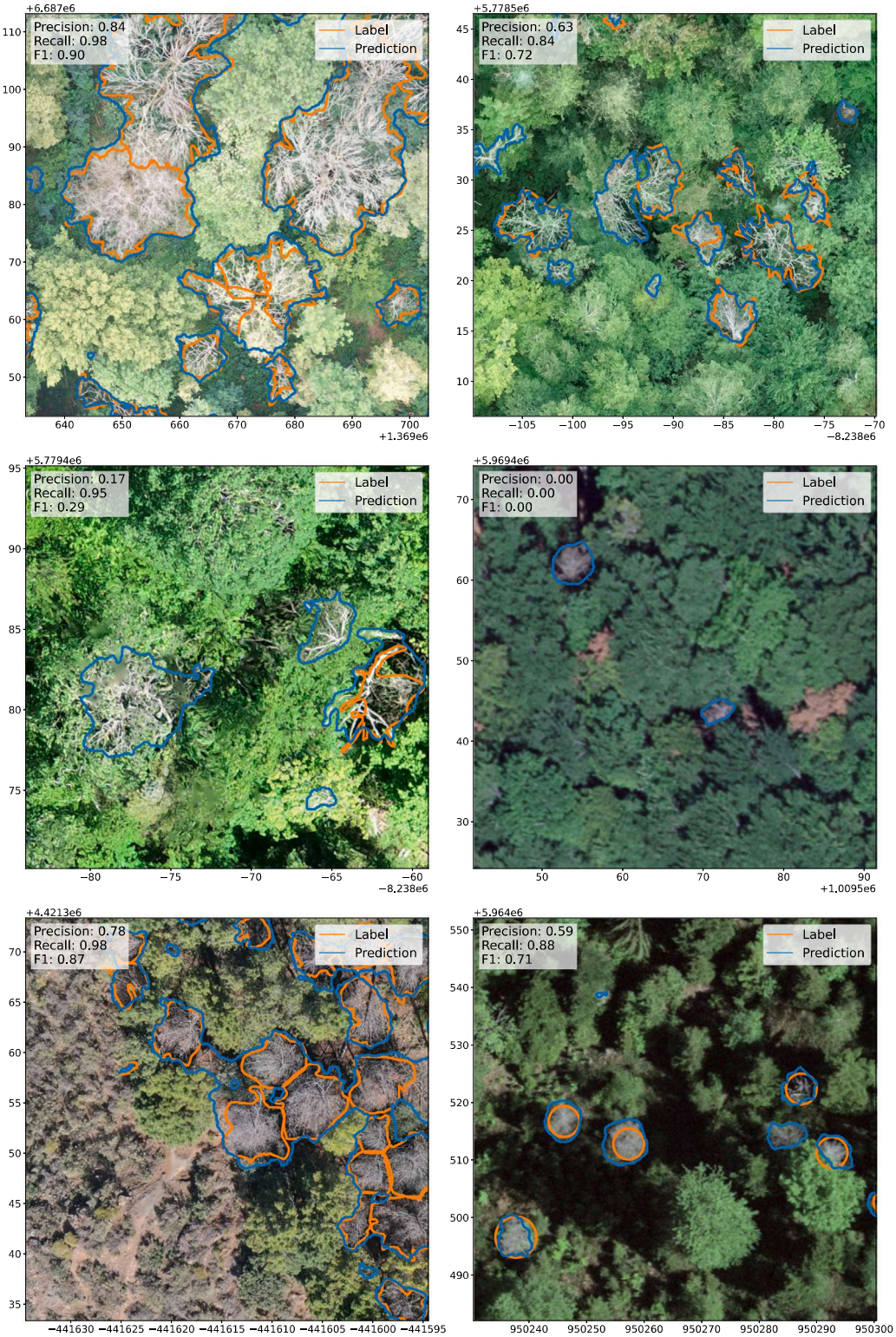

Fig. 5. Orthophotos from different biomes with predictions (blue) and manual labels (orange) with different label qualities. The noted precision, recall, and F1-score were computed for the respective displayed region. (For interpretation of the references to color in this figure legend, the reader is referred to the web version of this article.)

with continuous cover and lower structural diversity prevail, whereas in drylands and sub-tropical areas more vertically (subtropical) and horizontally (dryland) structured forests occur (Jucker et al., 2022).

The performance trends across resolutions (Fig. 4) as well as the number of tiles (Fig. 3) did not show entirely monotonic trends. For example, the performance in the (Sub) Tropical biome group for a resolution of 26 cm is better than for 24 cm. The underlying cause is that tile generation only includes down-sampling of orthophotos, meaning one orthophoto in a particular biome is only represented in the resolutions at or lower than its original resolution. Additionally,

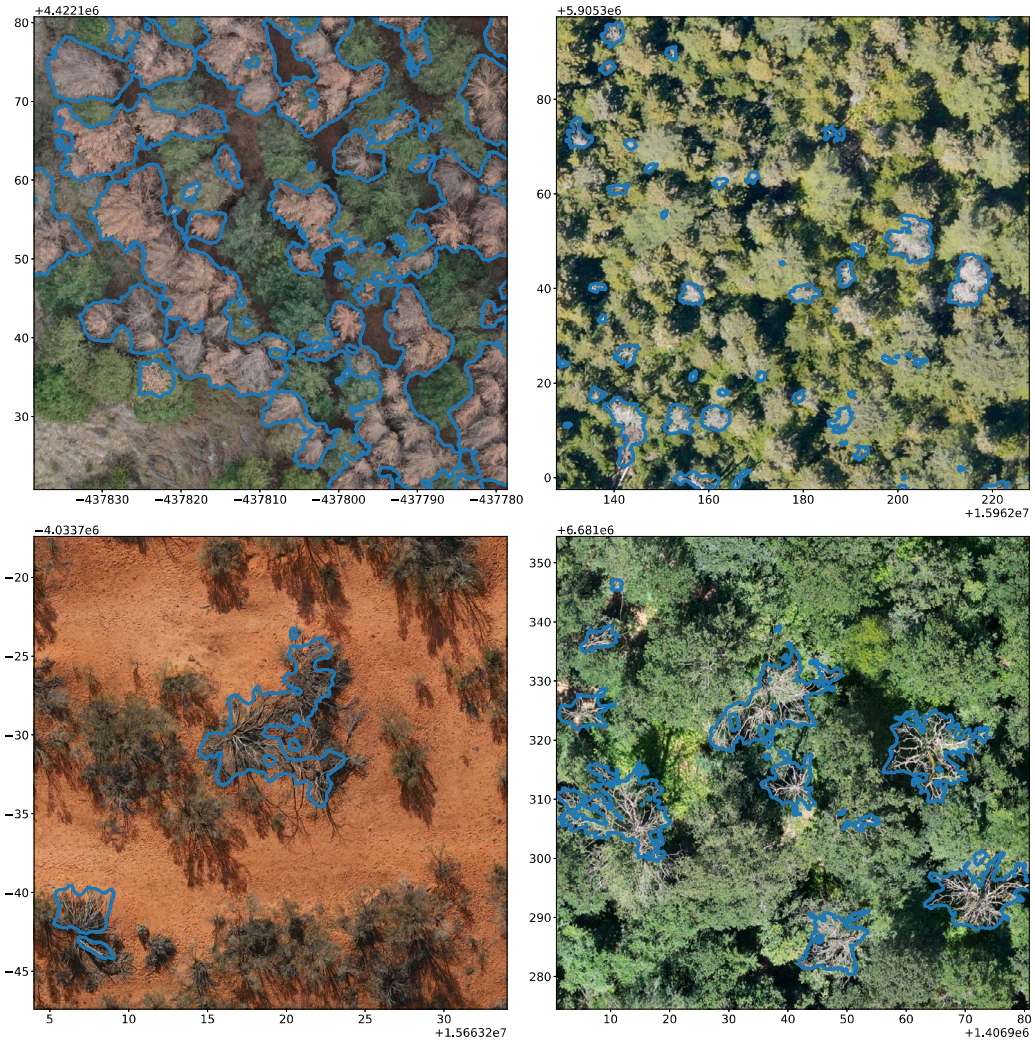

Fig. 6. Predictions in a diverse set of unlabeled high resolution orthophotos (<5 cm) across all forest biomes from the deadtrees.earth database (Mosig et al., 2024). Top Left: Andalusia (Spain). Top Right: Sakhalin Island (Russia). Bottom Left: South Australia (Australia). Bottom Right.: Saxony (Germany). Coordinate reference system is EPSG:3857 in meters.

the extent of an orthophoto determines the coarsest resolution of tiles that can be generated from it, considering tile size and the maximum fraction of no data values. This creates a natural resolution limit, resulting in fewer tiles at lower resolutions.

The model performance remains stable for lower resolutions in temperate and dryland biomes (Fig. 4). For boreal and tropical biomes the performance appears to decrease for lower image resolutions largely in synchrony with tile availability (Fig. 3). We argue that this decrease in performance does not reflect real-world settings but can be attributed to a small set of the same orthophotos that are downscaled to the respective resolutions (Table 1).

Compared to other studies on standing deadwood segmentation, such as Junttila et al. (2024) and Schiefer et al. (2023), the model performance appears low based on the F1-score alone. Here, visual inspection revealed that the key factor for comparably low performance scores was the variability in label accuracy across the crowd-sourced dataset (Fig. 5). The ability of the segmentation model to produce high precision values is directly correlated with the accuracy of the reference labels, reducing the overall F1-score, even when the model's predictions prove to be more accurate than the labels themselves or recover more partial dieback. In the nature of crowd-sourcing data, some contributions to the deadtrees.earth database clearly miss entire dead trees, and most commonly miss labels for partial dieback. These missing labels drastically decrease accuracy, resulting in a worse F1-score in the model evaluation, even when predictions are accurate. Fig. 5 demonstrates multiple examples of medium label quality leading to a low precision prediction, even though the segmented areas represent standing deadwood in the original image. Additionally, manually drawn polygons do not always precisely match the true tree crown contours; instead, they often approximate simpler polygons that may include areas beyond the crown. These labels inherently reduce precision when the model successfully segments individual tree crowns. Lastly, while label quality is relevant for any segmentation task, its relevance is amplified with segmentation tasks at high image resolutions. Despite this heterogeneity in label quality and its imprint on the model performance scores, the visual inspection revealed that the model still learned to accurately segment standing deadwood (Fig. 5).

Dead trees in the form of individual snags, while technically considered standing deadwood, are less likely to be detected by the model, as the provided labels primarily target fully and partially dead canopy.

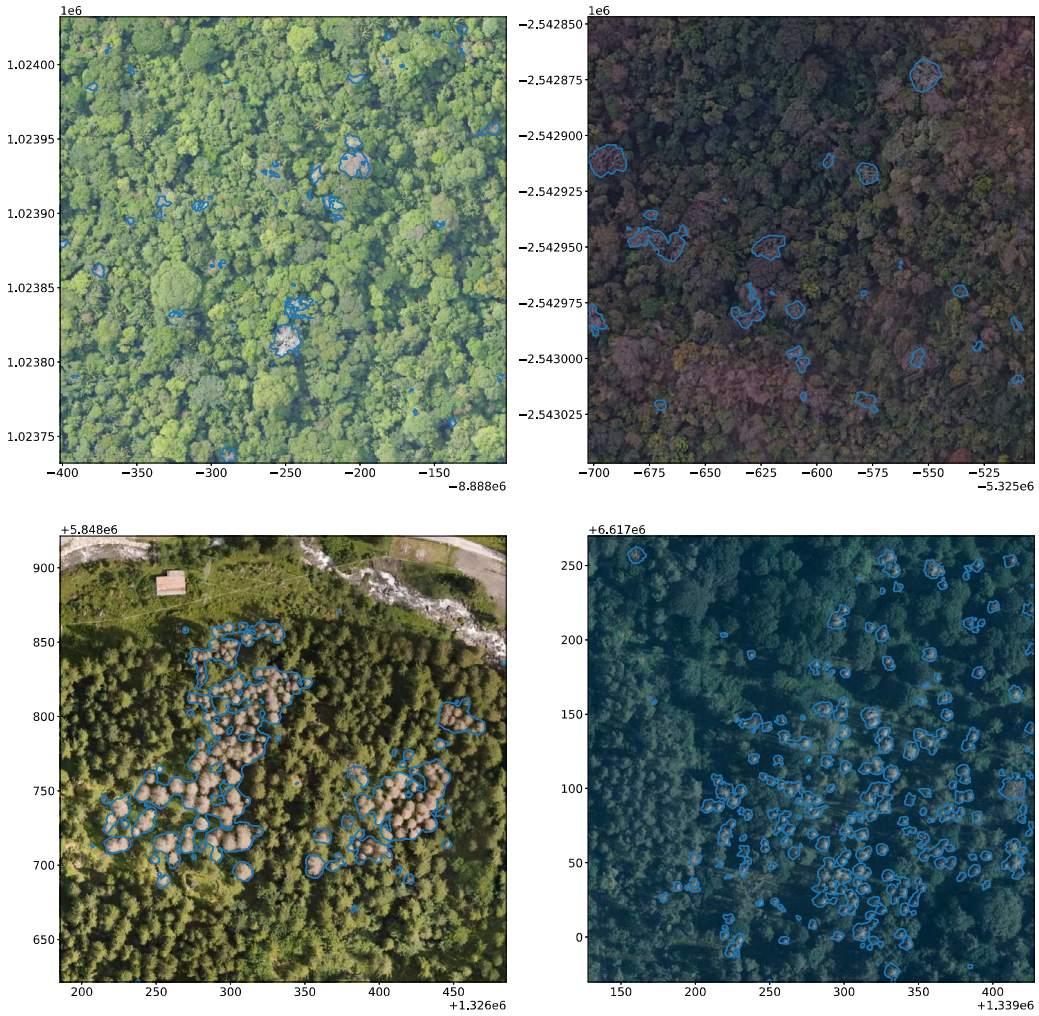

Fig. 7. Predictions in a set of low resolution orthophotos (>10 cm) across different forest biomes from the deadtrees.earth database (Mosig et al., 2024). Top Left: Barro Colorado Island, Panama. Top Right: Itirapina, Brazil. Bottom Left: Saxony, Germany. Bottom Right: Wetterzeube, Germany. Coordinate reference system is EPSG:3857 in meters.

Detecting such snags would likely require an airborne LiDAR-based approach, as demonstrated by Wing et al. (2015). However, this method is significantly more expensive than RGB-based alternatives and is also limited by the availability of reference data. Additionally, it is also important to emphasize that snags are generally of limited relevance for applied monitoring of tree mortality dynamics, as they can persist for decades and therefore may not represent recent mortality events or current forest health trends.

In this study, we trained a segmentation model for detecting fully dead tree crowns as well as partial canopy dieback across all forest biomes in varying resolutions. Training the model to generalize across multiple resolutions, the model must interpret full canopy mortality and partial dieback in varying levels of detail. Therefore, we trained the model at unprecedented image resolutions. While previous studies mostly focused on mapping tree mortality at coarse resolutions between 10–30 cm (Junttila et al., 2024; Schwarz et al., 2023; Cheng et al., 2024), here, we provide a model that can accurately detect standing deadwood from drone images with resolutions of a few centimeters to coarse representations as obtained from national airplane campaigns. To demonstrate the model's transferability to any orthophoto and any forest biome, we applied it to the entire orthophoto collection of deadtrees.earth. The resulting predictions are available and can be visualized as a vector layer on the website. A subset of the predictions is shown in Fig. 6 for high resolution imagery (<5 cm) and in Fig. 7 for lower resolution imagery (10 cm), illustrating that the model robustly handles diverse forest ecosystems, image resolutions, as well as partial and full dieback.

Considering the multi-resolution approach, the coverage across biomes and the multidimensional sampling scheme, computational complexity emerged as one of the biggest challenges. While the base imagery occupied 301 GiB of storage, the rescaled and tiled dataset occupied 943 GiB. Both tiles and the original images were compressed optimally with the DEFLATE algorithm. Given these constraints, we report results only for a SegFormer-based model and did not systematically benchmark alternative architectures or perform extensive hyperparameter optimization. Nevertheless, other state-of-the-art segmentation methods may prove promising in this context, including U-Net variants, DeepLabv3, HRNet (Ronneberger et al., 2015; Chen et al.,

2017; Wang et al., 2021). To facilitate such comparisons, we release the machine-learning-ready dataset, and we expect our SegFormer-based model to serve as a suitable baseline for future evaluations. We anticipate that community efforts leveraging this dataset will refine architectures and training regimes and further enhance monitoring of standing deadwood across biomes, resolutions, and forest types.

6. Conclusion & outlook

We trained and evaluated a deep learning-based pattern recognition model with a dataset covering all forest biomes and image resolutions from 1 cm to 28 cm to segment dead tree crowns as well as partial canopy dieback. We observed variations in segmentation performance between biomes and determined the optimal resolution for specific biomes. Given that our dataset is severely skewed in several dimensions, we implemented a four-dimensional sampling scheme to facilitate the development of a generalizing model. Our model's high quality and generalization ability were highlighted, as we observed qualitatively that the model output often segments standing deadwood more accurately than the crowd-sourced labels that the model was trained on. In the future, encoding additional metadata, such as biome, forest type, and resolution information, into the model encoder appears promising, as previous studies have demonstrated that integrating auxiliary information via a multi-modal approach can improve model performance (Heidarianbaei et al., 2024). Future model improvements will also build on the constantly increasing data availability of aerial imagery and corresponding labels at .

To the best of our knowledge, this is the first study to develop a method for mapping standing deadwood that is not limited to a specific biome or imagery resolution and can be applied across diverse forest ecosystems globally. For example, the model developed in this study can be directly used to assess the coverage of standing deadwood in any publicly available orthophotos, with resolutions finer than 30 cm, enabling large-scale monitoring of the standing deadwood across different landscapes. Further, we generated labels for the entire deadtrees.earth orthophoto database (Mosig et al., 2024) which now yields a globally accurate reference dataset of tree mortality. This could then be used as training data for satellite-based machine-learning models (Schiefer et al., 2023) or to evaluate existing products (Hansen et al., 2013; Senf et al., 2018). Our semantic segmentation model is tailored to aerial imagery with only RGB channels, as it is freely available from national aerial surveys or consumer-level drones. With these simple requirements based on the data presented in the segmentation approach, the corresponding straightforward applicability and scalability may be key to contributing to our understanding of tree mortality dynamics at global scales.

CRediT authorship contribution statement

Jakobus Möhring: Writing – review & editing, Writing – original draft, Visualization, Validation, Software, Methodology, Formal analysis, Data curation, Conceptualization. **Teja Kattenborn:** Writing – review & editing, Writing – original draft, Supervision, Project administration, Methodology, Investigation, Funding acquisition, Formal analysis, Data curation, Conceptualization. **Miguel D. Mahecha:** Writing – review & editing, Supervision, Methodology, Funding acquisition. **Yan Cheng:** Writing – review & editing, Validation, Methodology, Investigation, Data curation, Conceptualization. **Mirela Beloiu Schwenke:** Writing – review & editing, Data curation. **Myriam Cloutier:** Writing – review & editing, Data curation. **Martin Denter:** Writing – review & editing, Data curation. **Julian Frey:** Writing – review & editing, Data curation. **Matthias Gassilloud:** Writing – review & editing, Data curation. **Anna Göritz:** Writing – review & editing, Data curation. **Jan Hempel:** Data curation. **Stéphanie Horion:** Writing – review & editing, Data curation. **Tommaso Jucker:** Writing – review & editing, Data curation. **Samuli Junttila:** Writing – review & editing, Data curation. **Pratima Khatri-Chhetri:** Writing – review & editing, Data curation. **Kirill Korznikov:** Writing – review & editing, Data curation. **Stefan Kruse:** Writing – review & editing, Data curation. **Etienne Laliberté:** Writing – review & editing, Data curation. **Michael Maroschek:** Writing – review & editing, Data curation. **Paul Neumeier:** Data curation. **Oscar Pérez-Priego:** Writing – review & editing, Data curation. **Alastair Potts:** Writing – review & editing, Data curation. **Felix Schiefer:** Writing – review & editing, Data curation. **Rupert Seidl:** Writing – review & editing, Data curation. **Janusch Vajna-Jehle:** Writing – review & editing, Visualization, Validation, Software. **Katarzyna Zielewska-Büttner:** Writing – review & editing, Data curation. **Clemens Mosig:** Writing – review & editing, Writing – original draft, Visualization, Validation, Supervision, Software, Methodology, Investigation, Formal analysis, Data curation, Conceptualization.

Code availability

All code and ready-to-use models are available online. To reproduce the results in this paper: https://github.com/jmoeh/standing-deadwood. To apply the model to new orthophotos: https://github.com/cmosig/deadtreesmodels. A final model trained on the entire dataset is automatically applied to all uploaded orthophotos https://www.deadtrees.earth.

Declaration of competing interest

The authors declare that they have no known competing financial interests or personal relationships that could have appeared to influence the work reported in this paper.

Acknowledgments

The study is supported by the deadtrees initiative (https://www.deadtrees.earth). The deadtrees.earth initiative is supported by the Ministry for Food, Rural Areas, and Consumer Protection, Baden-Württemberg, Germany (grant 52-8670.00) and the German Research Foundation via the NFDI4Earth pilot project GeoLabel (DFG project no. 460036893, https://www.nfdi4earth.de/). CM, MDM and TK thank the European Space Agency, France for funding the "DeepFeatures" project via the AI4SCIENCE activity. CM and MDM thank the Federal Ministry for Economic Affairs and Climate Action, Germany for funding the project ML4Earth (FKZ 50EE2201B). TK acknowledges funding from the German Research Foundation (DFG) within the project PANOPS (project no. 504978936). MBS acknowledges funding from the Swiss National Science Foundation, United States (grant no.: https://www.mysnf.ch/grant.aspx?id=82ee2e84-bed0-4b15-9771-ea3271ee7240, IZCOZ0_213355). KK acknowledges the research grant 23-05272S of the Czech Science Foundation, Czechia. AG, MG received funding from the German Research Foundation (DFG) under the project ECOSENSE (SFB 1537/1).

Appendix

A.1. Biome aggregation

All original biomes by Olson et al. (2001) were aggregated in four distinct biome groups:

- **Boreal and Montane:** 'Boreal Forests/Taiga' and 'Montane Grasslands and Shrublands Tundra'
- **Drylands:** 'Mediterranean Forests, Woodlands, and Scrub', 'Deserts and Xeric Shrublands', and 'Flooded Grasslands and Savannas'
- **Temperate:** 'Temperate Broadleaf and Mixed Forests', 'Temperate Coniferous Forests', and 'Temperate Grasslands, Savannas, and Shrublands'

- **(Sub) Tropical:** 'Tropical and Subtropical Moist Broadleaf Forests', 'Tropical and Subtropical Dry Broadleaf Forests', 'Tropical and Subtropical Coniferous Forests', 'Tropical and Subtropical Grasslands, Savannas, and Shrublands', and 'Mangroves'

A.2. Acquisition date

For non-tropical regions, all orthophotos were captured during the leaf-on season of the respective biome, meaning all leafless branches and trees are standing deadwood. In tropical regions, the dataset contains orthophotos throughout the entire year, as there is no reliable phenological dataset that can be naively applied as a filter. While this means that not all leafless trees are standing deadwood, it is irrelevant to the successful training of a segmentation model.

Data availability

The entire dataset of manual labels and aerial imagery that were used in this study are available as orthophoto and tiled dataset on https://deadtrees.earth/.

References

Abraham, N., Khan, N.M., 2019. A novel focal tversky loss function with improved attention U-net for lesion segmentation. In: 2019 IEEE 16th International Symposium on Biomedical Imaging (ISBI 2019). IEEE, pp. 683–687. http://dx.doi.org/10.1109/isbi.2019.8759329.

Allen, C.D., Breshears, D.D., McDowell, N.G., 2015. On underestimation of global vulnerability to tree mortality and forest die-off from hotter drought in the anthropocene. Ecosphere 6 (8), 1–55. http://dx.doi.org/10.1890/ES15-00203.1.

Allen, M.J., Moreno-Fernández, D., Ruiz-Benito, P., Grieve, S.W., Lines, E.R., 2024. Low-cost tree crown dieback estimation using deep learning-based segmentation. Environ. Data Sci. 3, e18. http://dx.doi.org/10.1017/eds.2024.16.

Bradski, G., 2000. The OpenCV Library. Dr. Dobb's J. Softw. Tools.

Chen, L.-C., Papandreou, G., Schroff, F., Adam, H., 2017. Rethinking atrous convolution for semantic image segmentation. arXiv Preprint arXiv:1706.05587.

Cheng, Y., Oehmcke, S., Brandt, M., Rosenthal, L., Das, A., Vrieling, A., Saatchi, S., Wagner, F., Mugabowindekwe, M., Verbruggen, W., et al., 2024. Scattered tree death contributes to substantial forest loss in california. Nat. Commun. 15 (1), 641. http://dx.doi.org/10.1038/s41467-024-44991-z.

Denter, M., Frey, J., Kattenborn, T., Weinacker, H., Seifert, T., Koch, B., 2022. Assessment of camera focal length influence on canopy reconstruction quality. ISPRS Open J. Photogramm. Remote. Sens. 6, 100025. http://dx.doi.org/10.1016/j.ophoto.2022.100025.

Frey, J., Kovach, K., Stemmler, S., Koch, B., 2018. UAV photogrammetry of forests as a vulnerable process. a sensitivity analysis for a structure from motion RGB-image pipeline. Remote. Sens. 10 (6), 912. http://dx.doi.org/10.3390/rs10060912.

Gugger, S., Debut, L., Wolf, T., Schmid, P., Mueller, Z., Mangrulkar, S., Sun, M., Bossan, B., 2022. Accelerate: Training and inference at scale made simple, efficient and adaptable.. https://github.com/huggingface/accelerate.

Hansen, M.C., Potapov, P.V., Moore, R., Hancher, M., Turubanova, S.A., Tyukavina, A., Thau, D., Stehman, S.V., Goetz, S.J., Loveland, T.R., Kommareddy, A., Egorov, A., Chini, L., Justice, C.O., Townshend, J.R.G., 2013. High-resolution global maps of 21st-century forest cover change. Science 342 (6160), 850–853. http://dx.doi.org/10.1126/science.1244693.

Hartmann, H., Bastos, A., Das, A.J., Esquivel-Muelbert, A., Hammond, W.M., Martínez-Vilalta, J., McDowell, N.G., Powers, J.S., Pugh, T.A., Ruthrof, K.X., et al., 2022. Climate change risks to global forest health: emergence of unexpected events of elevated tree mortality worldwide. Annu. Rev. Plant Biology 73, 673–702. http://dx.doi.org/10.1146/annurev-arplant-102820-012804.

Heidarianbaei, M., Kanyamahanga, H., Dorozynski, M., 2024. Temporal vit-u-net tandem model: Enhancing multi-sensor land cover classification through transformer-based utilization of satellite image time series. ISPRS Ann. Photogramm. Remote. Sens. Spatial Inf. Sci. X-3-2024, 169–177. http://dx.doi.org/10.5194/isprs-annals-X-3-2024-169-2024, URL: https://isprs-annals.copernicus.org/articles/X-3-2024/169/2024/.

Iakubovskii, P., 2019. Segmentation models pytorch. https://github.com/qubvel/segmentation_models.pytorch,

Jadon, S., 2020. A survey of loss functions for semantic segmentation. In: 2020 IEEE Conference on Computational Intelligence in Bioinformatics and Computational Biology. CIBCB, pp. 1–7. http://dx.doi.org/10.1109/CIBCB48159.2020.9277638.

Jucker, T., Fischer, F.J., Chave, J., Coomes, D.A., Caspersen, J., Ali, A., Loubota Panzou, G.J., Feldpausch, T.R., Falster, D., Usoltsev, V.A., Adu-Bredu, S., Alves, L.F., Aminpour, M., Angoboy, I.B., Anten, N.P.R., Antin, C., Askari, Y., Muñoz, R., Ayyappan, N., Balvanera, P., Banin, L., Barbier, N., Battles, J.J., Beeckman, H., Bocko, Y.E., Bond-Lamberty, B., Bongers, F., Bowers, S., Brade, T., van Breugel, M., Chantrain, A., Chaudhary, R., Dai, J., Dalponte, M., Dimobe, K., Domec, J.-C., Doucet, J.-L., Duursma, R.A., Enríquez, M., van Ewijk, K.Y., Farfán-Rios, W., Fayolle, A., Forni, E., Forrester, D.I., Gilani, H., Godlee, J.L., Gourlet-Fleury, S., Haeni, M., Hall, J.S., He, J.-K., Hemp, A., Hernández-Stefanoni, J.L., Higgins, S.I., Holdaway, R.J., Hussain, K., Hutley, L.B., Ichie, T., Iida, Y., Jiang, H.-s., Joshi, P.R., Kaboli, H., Larsary, M.K., Kenzo, T., Kloeppel, B.D., Kohyama, T., Kunwar, S., Kuyah, S., Kvasnica, J., Lin, S., Lines, E.R., Liu, H., Lorimer, C., Loumeto, J.-J., Malhi, Y., Marshall, P.L., Mattsson, E., Matula, R., Meave, J.A., Mensah, S., Mi, X., Momo, S., Moncrieff, G.R., Mora, F., Nissanka, S.P., O'Hara, K.L., Pearce, S., Pelissier, R., Peri, P.L., Ploton, P., Poorter, L., Pour, M.J., Pourbabaei, H., Dupuy-Rada, J.M., Ribeiro, S.C., Ryan, C., Sanaei, A., Sanger, J., Schlund, M., Sellan, G., Shenkin, A., Sonké, B., Sterck, F.J., Svátek, M., Takagi, K., Trugman, A.T., Ullah, F., Vadeboncoeur, M.A., Valipour, A., Vanderwel, M.C., Vovides, A.G., Wang, W., Wang, L.-Q., Wirth, C., Woods, M., Xiang, W., Ximenes, F.d., Xu, Y., Yamada, T., Zavala, M.A., 2022. Tallo: A global tree allometry and crown architecture database. Global Change Biol. 28 (17), 5254–5268. http://dx.doi.org/10.1111/gcb.16302.

Jucker, T., Fischer, F.J., Chave, J., Coomes, D.A., Caspersen, J., Ali, A., Panzou, G.J.L., Feldpausch, T.R., Falster, D., Usoltsev, V.A., Jackson, T.D., Adu-Bredu, S., Alves, L.F., Aminpour, M., Angoboy, I.B., Anten, N.P.R., Antin, C., Askari, Y., Muñoz, R., Ayyappan, N., Banin, L., Barbier, N., Battles, J.J., Beeckman, H., Bocko, Y.E., Bond-Lamberty, B., Bongers, F., Bowers, S., van Breugel, M., Chantrain, A., Chaudhary, R., Dai, J., Dalponte, M., Dimobe, K., Domec, J.-C., Doucet, J.-L., Dupuy Rada, J.M., Duursma, R.A., Enríquez, M., van Ewijk, K.Y., Farfán-Rios, W., Fayolle, A., Ferretti, M., Forni, E., Forrester, D.I., Gilani, H., Godlee, J.L., Haeni, M., Hall, J.S., He, J.-K., Hemp, A., Hernández-Stefanoni, J.L., Higgins, S.I., Holdaway, R.J., Hussain, K., Hutley, L.B., Ichie, T., Iida, Y., Jiang, H.-s., Joshi, P.R., Kaboli, H., Larsary, M.K., Kenzo, T., Kloeppel, B.D., Kohyama, T., Kunwar, S., Kuyah, S., Kvasnica, J., Lin, S., Lines, E.R., Liu, H., Lorimer, C., Loumeto, J.-J., Malhi, Y., Marshall, P.L., Mattsson, E., Matula, R., Meave, J.A., Mensah, S., Mi, X., Momo, S.T., Moncrieff, G.R., Mora, F., Nissanka, S.P., Nur Hajar, Z.S., O'Hara, K.L., Pearce, S., Pelissier, R., Peri, P.L., Ploton, P., Poorter, L., Pour, M.J., Pourbabaei, H., Ribeiro, S.C., Ryan, C., Sanaei, A., Sanger, J., Schlund, M., Sellan, G., Shenkin, A., Sonké, B., Sterck, F.J., Svátek, M., Takagi, K., Trugman, A.T., Vadeboncoeur, M.A., Valipour, A., Vanderwel, M.C., Vovides, A.G., Waldner, P., Wang, W., Wang, L.-Q., Wirth, C., Woods, M., Xiang, W., de Aquino Ximenes, F., Xu, Y., Yamada, T., Zavala, M.A., Zimmermann, N.E., 2024. The global spectrum of tree crown architecture. http://dx.doi.org/10.1101/2024.09.14.613032, arXiv:https://www.biorxiv.org/content/early/2024/09/17/2024.09.14.613032.full.pdf URL: https://www.biorxiv.org/content/early/2024/09/17/2024.09.14.613032,

Junttila, S., Blomqvist, M., Laukkanen, V., Heinaro, E., Polvivaara, A., O'Sullivan, H., Yrttimaa, T., Vastaranta, M., Peltola, H., 2024. Significant increase in forest canopy mortality in boreal forests in southeast Finland. Forest Ecol. Manag. (ISSN: 0378-1127) 565, 122020. http://dx.doi.org/10.1016/j.foreco.2024.122020.

Kattenborn, T., Leitloff, J., Schiefer, F., Hinz, S., 2021. Review on convolutional neural networks (CNN) in vegetation remote sensing. ISPRS J. Photogramm. Remote Sens. 173, 24–49. http://dx.doi.org/10.1016/j.isprsjprs.2020.12.010.

Kattenborn, T., Schiefer, F., Frey, J., Feilhauer, H., Mahecha, M.D., Dormann, C.F., 2022. Spatially autocorrelated training and validation samples inflate performance assessment of convolutional neural networks. ISPRS Open J. Photogramm. Remote. Sens. 5, 100018. http://dx.doi.org/10.1016/j.ophoto.2022.100018.

Khatri-Chhetri, P., van Wagtendonk, L., Hendryx, S.M., Kane, V.R., 2024. Enhancing individual tree mortality mapping: The impact of models, data modalities, and classification taxonomy. Remote Sens. Environ. 300, 113914. http://dx.doi.org/10.1016/j.rse.2023.113914.

Loshchilov, I., 2017. Decoupled weight decay regularization. http://dx.doi.org/10.48550/arXiv.1711.05101, arXiv preprint arXiv:1711.05101.

Mosig, C., Vajna-Jehle, J., Mahecha, M.D., Cheng, Y., Hartmann, H., Montero, D., Junttila, S., Horion, S., Schwenke, M.B., Adu-Bredu, S., Al-Halbouni, D., Allen, M., Altman, J., Angiolini, C., Astrup, R., Barrasso, C., Bartholomeus, H., Brede, B., Buras, A., Carrieri, E., Chirici, G., Cloutier, M., Cushman, K., Dalling, J.W., Dempewolf, J., Denter, M., Ecke, S., Eichel, J., Eltner, A., Fabi, M., Fassnacht, F., Feirreira, M.P., Frey, J., Frick, A., Ganz, S., Garbarino, M., García, M., Gassilloud, M., Ghasemi, M., Giannetti, F., Gonzalez, R., Gosper, C., Greinwald, K., Grieve, S., Gutierrez, J.A., Göritz, A., Hajek, P., Hedding, D., Hempel, J., Hernández, M., Heurich, M., Honkavaara, E., Jucker, T., Kalwij, J.M., Khatri-Chhetri, P., Klemmt, H.-J., Koivumäki, N., Korznikov, K., Kruse, S., Krüger, R., Laliberté, E., Langan, L., Latifi, H., Lehmann, J., Li, L., Lines, E., Lopatin, J., Lucieer, A., Ludwig, M., Ludwig, A., Lyytikäinen-Saarenmaa, P., Ma, Q., Marino, G., Maroschek, M., Meloni, F., Menzel, A., Meyer, H., Miraki, M., Moreno-Fernández, D., Muller-Landau, H.C., Mälicke, M., Möhring, J., Müllerova, J., Neumeier, P., Näsi, R., Oppgenoorth, L., Palmer, M., Paul, T., Potts, A., Prober, S., Puliti, S., Pérez-Priego, O., Reudenbach, C., Rossi, C., Ruehr, N.K., Ruiz-Benito, P., Runge, C.M., Scherer-Lorenzen, M., Schiefer, F., Schladebach, J., Schmehl, M.-T., Schwarz, S., Seidl, R., Shafeian, E., de Simone, L., Sohrabi, H., Sotomayor, L., Sparrow, B.,

Steer, B.S., Stenson, M., Stöckigt, B., Su, Y., Suomalainen, J., Torresani, M., Umlauft, J., Vargas-Ramírez, N., Volpi, M., Vásquez, V., Weinstein, B., Ximena, T.C., Zdunic, K., Zielewska-Büttner, K., de Oliveira, R.A., van Wagtendonk, L., von Dosky, V., Kattenborn, T., 2024. Deadtrees.earth - an open-access and interactive database for centimeter-scale aerial imagery to uncover global tree mortality dynamics. http://dx.doi.org/10.1101/2024.10.18.619094, BioRxivarXiv:https://www.biorxiv.org/content/early/2024/10/20/2024.10.18.619094.1.full.pdf URL: https://www.biorxiv.org/content/early/2024/10/20/2024.10.18.619094.1.

Müller, D., Soto-Rey, I., Kramer, F., 2022. Towards a guideline for evaluation metrics in medical image segmentation. BMC Res. Notes (ISSN: 1756-0500) 15 (1), http://dx.doi.org/10.1186/s13104-022-06096-y.

Olson, D.M., Dinerstein, E., Wikramanayake, E.D., Burgess, N.D., Powell, G.V.N., Underwood, E.C., D'amico, J.A., Itoua, I., Strand, H.E., Morrison, J.C., Loucks, C.J., Allnutt, T.F., Ricketts, T.H., Kura, Y., Lamoreux, J.F., Wettengel, W.W., Hedao, P., Kassem, K.R., 2001. Terrestrial Ecoregions of the World: A New Map of Life on Earth: A new global map of terrestrial ecoregions provides an innovative tool for conserving biodiversity. BioScience (ISSN: 0006-3568) 51 (11), 933–938. http://dx.doi.org/10.1641/0006-3568(2001)051[0933:TEOTWA]2.0.CO;2, arXiv:https://academic.oup.com/bioscience/article-pdf/51/11/933/26890733/51-11-933.pdf URL: https://doi.org/10.1641/0006-3568(2001)051[0933:TEOTWA]2.0.CO;2.

Paszke, A., Gross, S., Massa, F., Lerer, A., Bradbury, J., Chanan, G., Killeen, T., Lin, Z., Gimelshein, N., Antiga, L., et al., 2019. Pytorch: An imperative style, high-performance deep learning library. Adv. Neural Inf. Process. Syst. 32, http://dx.doi.org/10.48550/arXiv.1912.01703.

Ronneberger, O., Fischer, P., Brox, T., 2015. U-net: Convolutional networks for biomedical image segmentation. http://dx.doi.org/10.1007/978-3-319-24574-4_28, arXiv:1505.04597 URL: https://arxiv.org/abs/1505.04597.

Schiefer, F., Kattenborn, T., Frick, A., Frey, J., Schall, P., Koch, B., Schmidtlein, S., 2020. Mapping forest tree species in high resolution UAV-based RGB-imagery by means of convolutional neural networks. ISPRS J. Photogramm. Remote Sens. 170, 205–215. http://dx.doi.org/10.1016/j.isprsjprs.2020.10.015.

Schiefer, F., Schmidtlein, S., Frick, A., Frey, J., Klinke, R., Zielewska-Büttner, K., Junttila, S., Uhl, A., Kattenborn, T., 2023. UAV-based reference data for the prediction of fractional cover of standing deadwood from sentinel time series. ISPRS Open J. Photogramm. Remote. Sens. 8, 100034. http://dx.doi.org/10.1016/j.ophoto.2023.100034.

Schwarz, S., Werner, C., Fassnacht, F.E., Ruehr, N.K., 2023. Forest canopy mortality during the 2018–2020 summer drought years in central europe: The application of a deep learning approach on aerial images across Luxembourg. In: Kattenborn, T. (Ed.), For.: An Int. J. For. Res. (ISSN: 1464-3626) 97 (3), 376–387. http://dx.doi.org/10.1093/forestry/cpad049.

Schwarz, S., Werner, C., Fassnacht, F.E., Ruehr, N.K., 2024. Forest canopy mortality during the 2018–2020 summer drought years in central europe: The application of a deep learning approach on aerial images across Luxembourg. For.: An Int. J. For. Res. 97 (3), 376–387. http://dx.doi.org/10.1093/forestry/cpad049.

Senf, C., Pflugmacher, D., Zhiqiang, Y., Sebald, J., Knorn, J., Neumann, M., Hostert, P., Seidl, R., 2018. Canopy mortality has doubled in europe's temperate forests over the last three decades. Nat. Commun. 9 (1), 4978. http://dx.doi.org/10.1038/s41467-018-07539-6.

The International Tree Mortality Network, Senf, C., Esquivel-Muelbert, A., Pugh, T.A.M., Anderegg, W.R.L., Anderson-Teixeira, K.J., Arellano, G., Beloiu Schwenke, M., Bentz, B.J., Boehmer, H.J., Bond-Lamberty, B., Bordin, K., Boson De Castro-Faria, A., Brearley, F.Q., Bussotti, F., Cailleret, M., Camarero, J.J., Chirici, G., Costa, F.R., Dalagnol, R., Davi, H., Davies, S.J., Delzon, S., Dhakal, B.P., Ferreira De Lima, R.A., Ferretti, M., Fontaine, J.B., Garbarino, M., De Gasper, A.L., Gessler, A., Gilbert, G., Godlee, J.L., Gonçalves, F.M.P., Govaere, L., Gutiérrez, A.G., Gómez Cardozo, E., Hammond, W.M., Henrik, H., Hobi, M.L., Holz, A., Homeier, J., Hovenden, M.J., Huang, C.-Y., Hérault, B., Jackson, T., Jucker, T., Jump, A.S., Junttila, S., Kattenborn, T., Klipel, J., Kotowska, M.M., Král, K., La Porta, N., Lopez-Toledo, L., López-Camacho, R., Maeda, E.E., Mallol Díaz, J., Martínez-Vilalta, J., Mcdowell, N., Moonlight, P.W., Mori, A.S., Muda, M.A., Mund, J.-P., Muscarella, R., Méndez-Toribio, M., Müller, S.C., Nagel, T.A., Neagu, S., Nock, C.A., O'Brien, M.J., Penuelas, J., Perry, G.L.W., Phillips, O.L., Posada, J.M., Rodrigues, R.R., Roman, A., Rousseau, G.X., Ruehr, N.K., Ruiz-Benito, P., Ruthrof, K.X., Salas-Eljatib, C., Bergamin, R.S., Scharnweber, T., Schelhaas, M.-J., Schuldt, B., Schwarz, S., Seidl, R., Shorohova, E., Silva, A.C., Sioen, G., Socha, J.a., Stereńczak, K., Stillhard, J., Stojanovic, D.B., Suvanto, S., Svoboda, M., Sánchez-Pinillos, M., Tanentzap, A.J., Taylor, A.R., Turini Farah, F., Vacchiano, G., Van Der Maaten, E., Van Der Maaten-Theunissen, M., Vibrans, A.C., Vilagrosa, A., Vilanova, E., Waser, L.T., Wiser, S.K., Yu, K., Zavala, M.A., Oliveira, L.Z., Zuleta, D., 2025. Towards a global understanding of tree mortality. New Phytol. http://dx.doi.org/10.1111/nph.20407.

Trumbore, S., Brando, P., Hartmann, H., 2015. Forest health and global change. Science 349 (6250), 814–818. http://dx.doi.org/10.1126/science.aac6759.

Veitch-Michaelis, J., Cottam, A., Schweizer, D., Broadbent, E., Dao, D., Zhang, C., Almeyda Zambrano, A., Max, S., 2024. OAM-TCD: A globally diverse dataset of high-resolution tree cover maps. In: Globerson, A., Mackey, L., Belgrave, D., Fan, A., Paquet, U., Tomczak, J., Zhang, C. (Eds.), Advances in Neural Information Processing Systems. 37, Curran Associates, Inc., pp. 49749–49767. http://dx.doi.org/10.48550/arXiv.2407.11743, URL: https://proceedings.neurips.cc/paper_files/paper/2024/file/58efdd77196fa8159062afa0408245da-Paper-Datasets_and_Benchmarks_Track.pdf.

Wang, J., Sun, K., Cheng, T., Jiang, B., Deng, C., Zhao, Y., Liu, D., Mu, Y., Tan, M., Wang, X., Liu, W., Xiao, B., 2021. Deep high-resolution representation learning for visual recognition. In: IEEE Transactions on Pattern Analysis and Machine Intelligence. 43, (10), IEEE, pp. 3349–3364.

Wing, B.M., Ritchie, M.W., Boston, K., Cohen, W.B., Olsen, M.J., 2015. Individual snag detection using neighborhood attribute filtered airborne lidar data. Remote Sens. Environ. (ISSN: 0034-4257) 163, 165–179. http://dx.doi.org/10.1016/j.rse.2015.03.013, URL: https://www.sciencedirect.com/science/article/pii/S0034425715001091.

Zielewska-Büttner, K., Adler, P., Kolbe, S., Beck, R., Ganter, L.M., Koch, B., Braunisch, V., 2020. Detection of standing deadwood from aerial imagery products: Two methods for addressing the bare ground misclassification issue. Forests (ISSN: 1999-4907) 11 (8), http://dx.doi.org/10.3390/f11080801, URL: https://www.mdpi.com/1999-4907/11/8/801.